

Structural characterisation of α -synuclein -membrane interactions and the resulting aggregation using small angle scattering

Céline Galvagnion,^{*,†} Abigail Barclay,[‡] Katarzyna Makasewicz,[¶] Frederik
Ravnkilde Marlet,[†] Martine Moulin,[§] Juliette Devos,[§] Sara Linse,[¶] Anne Martel,[§]
Lionel Porcar,[§] Emma Sparr,^{||} Martin Cramer Pedersen,[‡] Felix Roosen-Runge,[⊥]
Lise Arleth,[‡] and Alexander K. Buell^{*,#}

[†]*Department of Drug Design and Pharmacology, University of Copenhagen, 2100
Copenhagen, Denmark*

[‡]*Niels Bohr Institute, University of Copenhagen, 2100 Copenhagen, Denmark*

[¶]*Department of Biochemistry and Structural Biology, Lund University, SE22100 Lund,
Sweden*

[§]*Institut Laue-Langevin, 71 avenue des Martyrs, 38042 Grenoble, France*

^{||}*Division of Physical Chemistry, Center for Chemistry and Chemical Engineering, Lund
University, P.O. Box 124, SE-22100, Lund, Sweden*

[⊥]*Department of Biomedical Sciences and Biofilms Research Center for Biointerfaces,
Malmö University, Malmö, Sweden*

[#]*Department of Biotechnology and Biomedicine, Technical University of Denmark, 2800
Kgs. Lyngby, Denmark*

E-mail: celine.galvagnion@sund.ku.dk; alebu@dtu.de

Abstract

The presence of amyloid fibrils is a hallmark of several neurodegenerative diseases. Some amyloidogenic proteins, such as α -synuclein and amyloid β , can interact with lipids, and this interaction can strongly favor the formation of amyloid fibrils. In particular the primary nucleation step, i.e. the *de novo* formation of amyloid fibrils, has been shown to be accelerated by lipids. However, the exact mechanism of this acceleration is still mostly unclear. Here we use a range of scattering methods, such as dynamic light scattering (DLS) and small angle X-ray and neutron scattering (SAXS and SANS) to obtain structural information on the binding of α -synuclein to vesicles formed from negatively charged lipids and their co-assembly into amyloid fibrils. We find that the lipid vesicles do not simply act as a surface that catalyses the nucleation reaction, but that lipid molecules take an active role in the reaction. The binding of α -synuclein to the lipid vesicles immediately induces a major structural change in the lipid assembly, which leads to a break-up into small, cylindrical and disc-like lipid-protein particles. This transition can be largely reversed by temperature changes or proteolytic protein removal. Incubation of these small, cylindrical and disc-like lipid- α -synuclein particles for several hours, however, yields amyloid fibril formation, whereby the lipids are incorporated into the fibrils.

Introduction

Protein aggregation into ordered fibrillar structures, amyloid fibrils, is a hallmark of a range of severe disorders, such as Alzheimer's, Parkinson's and the prion diseases.¹ α -synuclein is a small highly conserved pre-synaptic protein proposed to be involved in synaptic plasticity and whose aggregation into amyloid fibrils is the hallmark of Parkinson's disease.^{2,3} α -synuclein is natively disordered in solution,^{4,5} but in the presence of lipid bilayers and various surfactants the protein has been shown to adopt an α -helical conformation⁶ which is proposed to be important for its biological role.⁷ It has been known for about two decades that interactions between α -synuclein and lipid bilayers influence the kinetics of amyloid

formation of this protein.^{8,9}

α -synuclein:lipid mixtures can adopt a wide variety of structures whose dimensions and morphologies depend on the lipid-to-protein ratio and the charge, phase state and shape (vesicles vs. supported bilayer) of the lipid system as well as the aggregation state of α -synuclein. The observed structures range from an anchored protein shell around a lipid vesicle,¹⁰ to disintegrated vesicles,¹¹ tubular micelles,¹²⁻¹⁵ small lipid-protein nanoparticles¹⁶ and nanodiscs.^{17,18} Oligomeric assemblies of α -synuclein have also been found to permeabilize lipid bilayers.¹⁹⁻²¹ The binding affinity of α -synuclein to lipid bilayers is to a large extent determined by the negative charge density of the bilayer,¹⁸ because the positively charged N-terminal region of the protein drives the interaction.⁶ At high lipid-to-protein ratios, amyloid fibril formation is often suppressed, because the equilibrium is shifted towards the membrane-bound state, whereas at an excess of protein, amyloid fibril formation can be very significantly accelerated by the presence of lipid vesicles.²² It is becoming increasingly clear that in such cases, lipid molecules can become incorporated into the growing amyloid fibrils.^{23,24} The first atomic resolution structure of α -synuclein amyloid fibrils formed in the presence of lipids confirmed the presence of lipid molecules in the fibrils.²⁵ Despite the significant body of work that has been dedicated to α -synuclein-lipid interactions, the mechanistic steps of how interactions with lipids enable and accelerate amyloid fibril formation are still unresolved.

In recent years, we have developed a uniquely quantitative α -synuclein-lipid system that is particularly suitable to address these questions.^{22,24,26} Using a combination of kinetic analysis and systematic variation of the concentrations of lipids and monomeric protein in kinetic experiments of α -synuclein aggregation, it has been possible to quantitatively determine the contribution of negatively charged model membranes on α -synuclein aggregation. The role of the model membranes consists almost exclusively in an increase of the rate of primary nucleation by three orders of magnitude or more,²² compared to the aggregation under otherwise identical conditions but in the absence of lipids. This effect is only observed in the presence of an excess of protein, such as to completely saturate the high affinity ($K_D < 1 \mu\text{M}$) lipid

vesicles, while still having unbound protein free in solution. In these experiments, it was observed that the aggregation reaction stops before all the soluble protein is consumed. The thermodynamic stability of amyloid fibrils with respect to the soluble state is high^{27,28} and the equilibrium solubility of α -synuclein is often less than 1 μM .²⁹ However, under quiescent conditions at moderate temperatures in the presence of negatively charged lipid vesicles, the proportion of protein converted into amyloid fibrils is proportional to the initial quantity of added lipid vesicles and in some cases several tens of μM of soluble protein can be present in the plateau phase. This finding suggests that both nucleation and growth of fibrils eventually cease and even that the lipids behave as a reagent that is consumed, rather than a mere catalyst on the surface of which the aggregation processes occur. Our recent solid state Nuclear Magnetic Resonance investigation of the same α -synuclein-lipid system indeed showed that the dynamics of the lipid molecules are affected by the aggregation process, supporting the formation of lipid-protein co-aggregates.²⁴

In the present study, we aim to elucidate the role of lipids in the interaction with α -synuclein, which ultimately leads to the formation of kinetically trapped fibrils.²² In particular, our goal is to study the structural changes that the lipid vesicles undergo upon the binding of α -synuclein and the subsequent protein-lipid co-assembly. The length scales of the expected changes in lipid arrangement and structure are in the range of several nm or smaller, and hence not easily accessible to direct imaging techniques. Here, we report on the results of a detailed study of different lipid: α -synuclein systems by small-angle X-ray and neutron scattering (SAXS and SANS, respectively) techniques that allow the structural characterisation of the system on the relevant length scales. We employ a powerful combination of SANS and SAXS methods. SANS allows the study of lipid and protein components separately through contrast-variation techniques whereas SAXS enables a kinetic investigation of down to millisecond time scales through stopped-flow SAXS³⁰ as well as a larger q -range in a single setting. Contrast-variation techniques exploit that ^1H and ^2H (D) have very different scattering lengths for neutrons. By adjusting the H_2O to D_2O ratio of the aqueous solvent,

individual types or classes of molecules, such as proteins or lipids, can be matched out, i.e. selectively rendered invisible.³¹ Our DLS and SAXS/SANS measurements combined with data modelling show that the binding of α -synuclein to 1,2-dilauroyl-sn-glycero-3-phospho-L-serine (DLPS) or 1,2-dimyristoyl-sn-glycero-3-phospho-L-serine (DMPS) vesicles leads to a fast (less than 1 ms) and an almost fully reversible break-up of the lipid vesicles into small structures, including nanodiscs and rods. Moreover, our contrast-matching SANS measurements indicate that this fast reversible break-up of the vesicles upon α -synuclein binding is followed by lipid-protein co-aggregation. The SANS signature of the lipid is compatible with a systematic incorporation of lipid molecules into the protein fibrils. These results shed light onto the structural details of the lipid-protein structures formed by α -synuclein and are relevant to understand the cytotoxicity of the protein via membrane damage and the formation of pathological lipid-protein assemblies *in vivo*.³²

Results and discussion

The binding of α -synuclein to lipid vesicles leads to a structural rearrangement into small discs

We first used small angle X-ray scattering to investigate the structural details of the interaction between small unilamellar vesicles made with either DLPS or DMPS and α -synuclein. In particular, we mixed two solutions containing the vesicles and α -synuclein, respectively, at temperatures above the melting points of the lipids (i.e. 30°C and 45°C for DLPS and DMPS, respectively) and we acquired the X-ray scattering intensity in a q range of 0.006 to 0.35 \AA^{-1} (Figure 1 A,B). We observed that the X-ray scattering signature of DLPS and DMPS vesicles changed upon binding of α -synuclein. In particular, we observed that the binding of α -synuclein to the vesicles led to the loss of the oscillations of the scattering intensity of DLPS vesicles at low- q , a decrease of the scattering intensity from both DLPS

and DMPS vesicles at the lowest- q and a shift of the first minimum in the scattering profile to higher q -values. These results suggest that the vesicles undergo significant structural re-arrangements in terms of average size and bilayer thickness upon binding of α -synuclein.

We investigated the structural re-arrangement of the vesicles using both the pair-distance

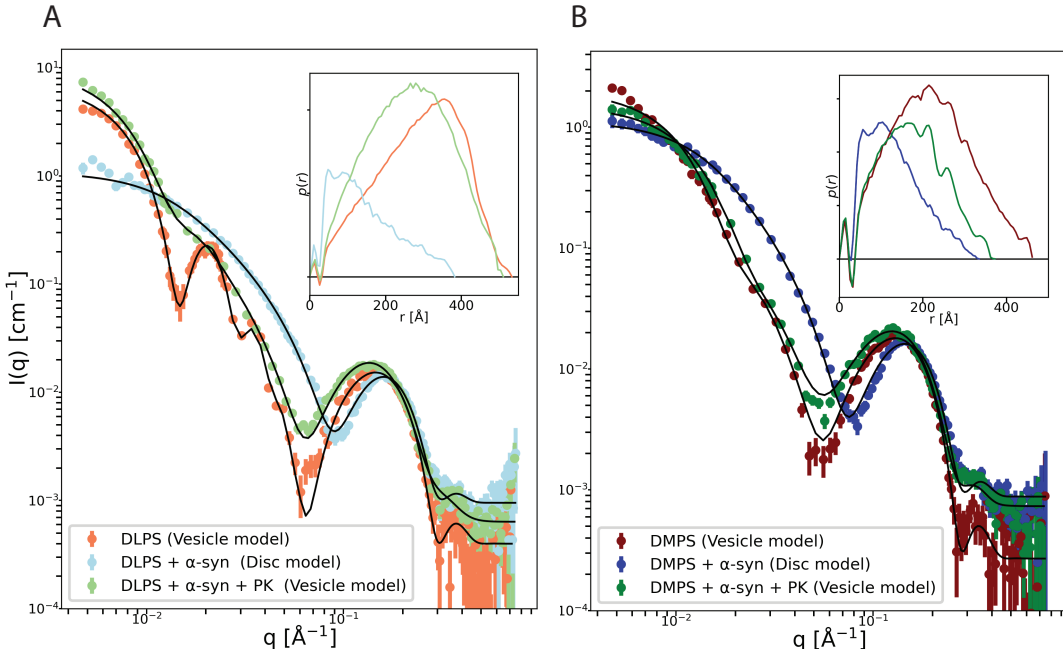


Figure 1: Structural characterisation of the system of α -synuclein:vesicles using SAXS. X-ray scattering profiles of 8 mM (A) DLPS and (B) DMPS vesicles incubated in the absence (orange/red) and the presence of $270 \mu\text{M}$ α -synuclein (blue) as well as after treatment with proteinase K (PK) (green). Model fits to the data are shown in black. Each PK treatment corresponds to incubation with $15.7 \mu\text{M}$ PK for 1 h at 37°C . The data were measured in phosphate buffer pH 6.5 at 30°C (A, DLPS) or 45°C (B, DMPS). The inserts show the $p(r)$ -distribution profiles generated from the SAXS data.

distribution profiles and modelling. The $p(r)$ -distribution profiles of the pure DMPS and DLPS vesicles (see insets to Figure 1 A and B) are representative of large vesicles. This is particularly clear from the typical almost-triangular shape of the DLPS data set. The initial fluctuation close to $r = 40 \text{\AA}$ represents structural properties of the lipid bilayer for core-shell structures and arises due to the presence of lipid headgroups and alkyl chains, which have positive and negative excess X-ray scattering lengths, respectively. In the presence of α -synuclein, however, the $p(r)$ distribution profiles are skewed / shifted to the left with a

broad cap and a tail on the right side, which is indicative of disc-like particles³³.

To gain deeper insights into the structural transformations apparent in these data we continue the analysis with a direct model-based approach. Our analytical models represent the lipid and lipid- α -synuclein structures as simple geometrical objects using form factors which can be found in the literature³⁴. Key information about the overall size and shape of the structures can be refined from the SAS data. The models were implemented in *WillItFit*³⁵ (see detailed descriptions of the models used in the SI).

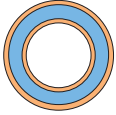
Importantly, to constrain the solution-space of the models and ensure the obtained solution is physically feasible, we incorporate chemical and biophysical information. The scattering lengths and molecular volumes assigned to each part of the model are preset according to which component(s) of the sample they represent (see supplementary table S1).

Additionally, the models are calculated on absolute scale by exploiting the lipid concentration of each sample to give even more convincing model calculations. In SAXS, fine tuning the molecular volumes of the various components can correct for small errors on the absolute scale. For larger deviations in absolute intensity between the data and our theoretical model calculations, a free scale parameter can be employed. This free parameter may account for errors in the absolute scaling of the data, as well as uncertainties in calculating the necessary contrasts and concentrations for the models.

A polydisperse three-shell vesicle model (Figure S7), where the three shells represent the outer lipid headgroups, tailgroups, and inner headgroups respectively, provides excellent fits to the SAXS data from pure DMPS and DLPS (Figure 1 A and B) while maintaining reasonable structural parameters, listed in Table 1. Size variation is taken into account by assuming a Gaussian distribution of sizes and fitting the mean radius as well as the standard deviation of radii. The lipid volumes V_{lipid} stay close to the starting values previously determined in the literature: 912 \AA^3 for DLPS³⁶ and 978 \AA^3 for DMPS³⁷. The area per lipid headgroup (A_{head}) can be deduced from the model fit results as $V_{\text{lipid}} / t_{\text{lipid}}$ with the thickness of one lipid leaflet t_{lipid} . For DLPS A_{head} lies around 55 \AA^2 , which is in close agreement

with the reports by Szekely *et al.* who found A_{head} to be 60.5 \AA^2 for DLPS in the fluid phase. For DMPS we find $A_{\text{head}} \sim 58 \text{ \AA}^2$, which we compare to the estimated value of 55.6 \AA^2 for DMPS in the fluid phase²⁶. The obtained radii of the vesicles between 130 (DMPS) and 210 (DLPS) \AA is reasonable with respect to the extrusion preparation, and shows a small polydispersity, characterized via a relative standard deviation σ_{Radius} between 10% (DLPS) and 30% (DMPS).

Table 1: Structural parameters refined from the SAXS data of DMPS and DLPS vesicles shown in Figure 1 A and B using the Three-shell vesicle model. The model was calculated on absolute scale. *Parameter was fixed during refinement. - means the parameter was not required to describe that data set.



	Parameter	DLPS	DMPS
	Scale	1*	1*
	Radius [\AA]	211 ± 5	128 ± 12
	σ_{Radius}	0.11 ± 0.002	0.35 ± 0.06
	V_{lipid} [\AA^3]	958 ± 3	1071 ± 3
	t_{lipid} [\AA]	17.4 ± 0.4	18.4 ± 0.3
	Roughness [\AA]	4.23 ± 0.34	4.71 ± 0.29
	Background [cm^{-1}]	0.004 ± 0.0003	0.0003 ± 0.0003
	χ^2	2.47	2.34

For both the DLPS- α -synuclein and the DMPS- α -synuclein mixtures, the $p(r)$ -distributions hold a close resemblance to that of a disc-like structure³³. We thus propose a scheme where the binding of α -synuclein leads to the deformation of vesicles into discoidal bilayer patches, which are stabilized by a belt of α -synuclein, in a similar manner as the one that amphipathic membrane scaffold proteins can stabilize lipid nanodiscs^{16,38} (Figure S8). Our analytical model builds upon our previously developed model for nanodiscs^{39,40} where the lipid bilayer is described as a collection of discs. Each disc represents the lipid headgroups, tailgroups and protein belts, respectively. Here we alter the volumes and scattering lengths assigned to each disc, in order to additionally allow the amphipathic N-terminal and hydrophobic regions of α -synuclein to be accounted for in the lipid bilayer. The hydrophilic C-terminal tails of α -synuclein, which are thought to remain disordered, protrude from the outside of the disc as Gaussian random coils, following the same modelling strategy as presented by Arleth *et al.*⁴¹ (see more details in the SI 'Disc with Gaussian random coils' model).

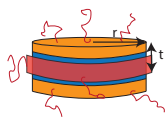
The 'Disc with Gaussian random coils' model provides good fits to the data for both

DLPS and DMPS in the presence of α -synuclein (Figure 1). The model captures the low- q slopes of the scattering profiles accurately indicating that the overall shape and dimensions are well-described (see fit parameters in Table 2). We assume all of the protein is bound to the lipids since the DLPS and DMPS bilayers are in the fluid phase under the experimental conditions used here, and hence take a molar ratio of 30:1 lipid:protein (L/P) into account²⁶ when calculating scattering length densities of the discoidal bilayer. For these refinements it was necessary to fit a constant scale factor to the model rather than keeping the scale factor at unity. This scale factor could reflect uncertainty in determining the particle number density of the lipid- α -synuclein mixture with the model. Throughout this study, our modelling scheme has difficulties to accurately capture the dimensions of the protein. Therefore the radius of gyration $R_{g\ \alpha-syn}$ of the random coils was fixed to 18 Å, as calculated by Kohn's power law relationship for 44 amino acids,⁴² the length of the C-terminal tail of α -synuclein that does not interact with the lipid bilayer⁶(see SI for more details). Similarly we found the width of the protein belt, w_{belt} , did not have much influence on the shape of the model profile and was poorly determined as it is closely correlated with the free scale parameter. Therefore w_{belt} was fixed to the diameter of an α -helix, 12Å, under the plausible assumption that α -synuclein forms a helical structure upon binding.⁶ For both the DLPS- and DMPS- α -synuclein mixtures, we refine populations of polydisperse discs with mean radii of around 140 Å. The thickness of the bilayer was found to be identical within error to the dimensions refined from the pure lipid vesicle data in Table 1.

We note that we attempted to model these data as a range of different shapes and structures, including vesicles, cylinders and ribbons, but we were not able to match the scattering profile at low- q successfully with such alternative models. We also tried to model the data with variations of the disc model, including bicelles where the protein belt and random coils were not present, but found that our 'Disc with Gaussian random coils' captures all the features of the experimental profile the most accurately.

All together these SAXS measurements analysed using a direct model-based approach show

Table 2: Structural parameters refined from the SAXS data of DLPS- and DMPS- α -synuclein mixtures shown in Figure 1 using the 'Disc with Gaussian random coil' model. *Parameter was fixed during refinement.



	Parameters	DLPS + α -synuclein	DMPS + α -syn
	Scale	0.57 ± 0.56	0.87 ± 0.64
	L/P	30*	30*
	w_{Belt} [\AA]	12*	12*
	$R_{\text{g, } \alpha\text{-syn}}$ [\AA]	18*	18*
	Radius [\AA]	146 ± 69	136 ± 46
	σ_{Radius}	0.28 ± 0.01	0.26 ± 0.02
	V_{lipid} [\AA^3]	878 ± 36	937 ± 27
	$V_{\alpha\text{-syn}}$ [\AA^3]	21300 ± 1780	21200 ± 1420
	t_{lipid} [\AA]	18.8 ± 2.4	19.6 ± 1.6
	Roughness [\AA]	4.00 ± 2.42	4.19 ± 1.80
	Background [cm^{-1}]	0.001 ± 0.0004	0.0009 ± 0.0003
	χ^2	2.42	3.55

that the binding of α -synuclein to DMPS and DLPS vesicles leads to the break-up of the vesicles into small discs.

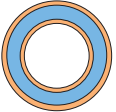
The structural re-arrangement of DLPS and DMPS vesicles into discs upon α -synuclein binding occurs on a millisecond timescale

We used stopped-flow SAXS (SF-SAXS) to investigate the time scale of the observed structural re-arrangement of DLPS and DMPS vesicles upon binding of α -synuclein. Figure 2 A,B show the X-ray scattering intensity at a q range of 0.006 to 0.35 \AA^{-1} during the first milliseconds after mixing DLPS or DMPS vesicles with buffer (0 ms) or α -synuclein (1-21 ms) at 30°C (Figure 2 A,B and S1). The SAXS data of the DLPS and DMPS vesicles (0 ms) were well-described by the polydisperse three-shell vesicle model whereas those of the protein-lipid mixtures acquired at 1 ms and later were described by the 'Disc with Gaussian random coils' model (see Figure S2 and Tables 3 and 4). This suggests that the structural re-arrangement of DLPS and DMPS vesicles into discs upon binding of α -synuclein takes place very fast within less than 1 ms, the dead-time of the stopped-flow setup,⁴³ thereby preventing a more precise analysis of the kinetics of the interaction.

In an attempt to rationalize the fast binding kinetics, we can model the binding of monomeric α -synuclein to the surface of lipid vesicles as a process of ligand binding to a fully absorbing

sphere, i.e. every diffusive encounter yields a binding event. We can calculate the diffusion-limited rate at steady state, according to $\frac{dn}{dt} = 4\pi DRc$,⁴⁴ where n is the number of bound molecules, D is the diffusion coefficient of the protein ($8.2 \cdot 10^{-11} \text{ m}^2\text{s}^{-1}$ for α -synuclein⁴⁵), R is the radius of the vesicle and c is α -synuclein concentration. At $c = 70 \mu\text{M}$, we obtain $\frac{dn}{dt} \approx 6.5 \cdot 10^5 \text{ s}^{-1}$. A vesicle with a radius of 15 nm contains of the order of 10,000 lipid molecules, if we consider a surface area per lipid of 55.6 \AA^2 , which translates into approximately 300 molecules of α -synuclein per vesicle at full saturation.²⁶ At a constant rate of binding, the vesicle would therefore be saturated after 0.5 ms. In reality the rate of binding will slow down, as more and more binding sites are occupied. However, this simple estimate shows that the observed rate of interaction between α -synuclein, and DMPS and DLPS vesicles at 30°C is probably close to the diffusion limit, despite the fact that the lipid vesicles and the α -synuclein both carry a net negative charge, which has the potential to reduce the maximal possible rate of binding due to electrostatic repulsive interactions. However, it is possible that the binding reaction is even electrostatically enhanced⁴⁶ once the α -synuclein molecule is close enough to the negatively charged vesicle, because it interacts with the N-terminus which carries a net positive charge.

Table 3: Structural parameters refined from the SAXS data in Figure S2 using the Three-shell vesicle model. We note that it was not possible to convert this data set to absolute scaling units and the model therefore requires a free Scale parameter far from 1.

	Parameters	DLPS (0ms)	DMPS (0ms)
	Scale	0.13 ± 0.51	0.12 ± 0.09
	Radius [\AA]	259 ± 16	534 ± 44
	σ_{Radius}	0.17 ± 0.06	0.23 ± 0.01
	v_{lipid} [\AA^3]	949 ± 147	1003 ± 40
	t_{lipid} [\AA]	17.9 ± 10.5	23.4 ± 2.6
	Roughness [\AA]	3.97 ± 10.7	3.94 ± 4.24
	Background [cm^{-1}]	0.0003 ± 0.0001	0.0002 ± 0.0001
	χ^2	2.47	6.26

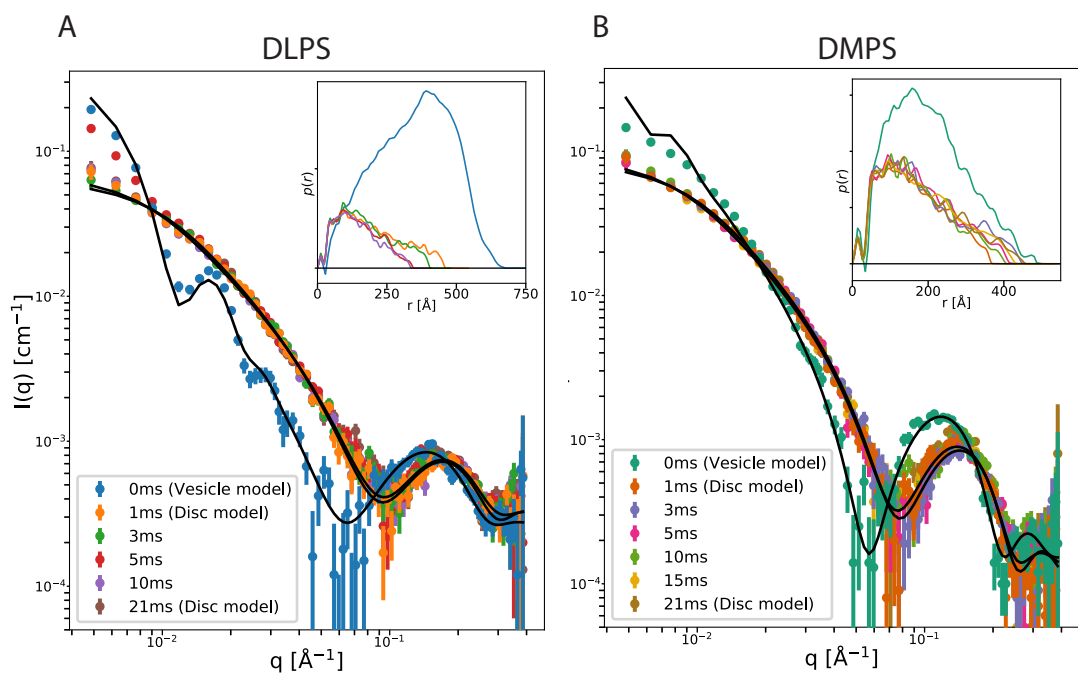
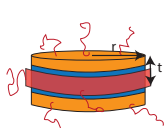


Figure 2: Characterisation of the kinetics and structural details of α -synuclein:vesicle interactions using stopped-flow SAXS. X-ray scattering function of a solution containing either (A) DLPS or (B) DMPS vesicles of 2 mM lipids and 70 μ M α -synuclein, measured at different time points after mixing. The solution conditions were 20 mM sodium phosphate buffer at pH 6.5 and 30°C. Insets show the $p(r)$ distribution profiles generated from the data.

Table 4: Structural parameters refined from the SAXS data in Figure S2 using the Disc with Gaussian random coil model. *Parameters fixed during refinement. We note that it was not possible to convert this data set to absolute scaling units and the model therefore requires a free Scale parameter significantly smaller than 1.



	Parameters	DLPS + α -syn (1ms)	DLPS + α -syn (21ms)	DMPS + α -syn (1ms)	DMPS + α -syn (21ms)
	Scale	0.03 ± 0.19	0.03 ± 0.07	0.06 ± 0.1	0.06 ± 0.12
	L/P	30*	30*	30*	30*
	w_{belt} [Å]	12*	12*	12*	12*
	$R_g \alpha\text{-syn}$ [Å]	18*	18*	18*	18*
	Radius [Å]	197 ± 163	174 ± 142	209 ± 154	189 ± 135
	σ_{Radius}	0.29 ± 0.03	0.28 ± 0.03	0.29 ± 0.02	0.28 ± 0.02
	v_{lipid} [Å ³]	858 ± 247	843 ± 173	937 ± 98	929 ± 98
	$v_{\alpha\text{-syn}}$ [Å ³]	18800 ± 11900	19000 ± 10600	19600 ± 7110	19600 ± 7110
	t_{lipid} [Å]	18.4 ± 15	19.2 ± 2.7	21.6 ± 6.2	21.9 ± 4.1
	Roughness [Å]	2.49 ± 22	0*	3.57 ± 8.80	2.42 ± 9.29
	Background [cm ⁻¹]	0.0003 ± 0.0002	0.0003 ± 0.0002	0.0001 ± 0.0001	0.0001 ± 0.0001
	χ^2	1.11	1.36	0.84	1.35

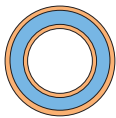
The structural re-arrangement of DLPS and DMPS vesicles into discs upon α -synuclein binding is reversible

Next, we investigated whether the structural changes that the vesicles undergo upon α -synuclein binding are reversible. To this end, it was necessary to analyze the structures of the vesicles after removing the protein. The high affinity between α -synuclein and DLPS or DMPS vesicles renders it difficult to completely remove the protein on a short time scale. We therefore designed an experimental protocol, whereby α -synuclein was digested with proteinase K (PK). To test the efficacy of this treatment, we performed differential scanning calorimetry (DSC) measurements of the α -synuclein-vesicle mixture before and after incubation with PK while exploiting the known effect of α -synuclein binding on the melting temperature (T_m) of the DMPS bilayer, i.e. $T_{m, \text{DMPS}} \sim 40^\circ\text{C}$ whereas $T_{m, \text{DMPS}:\alpha\text{-synuclein}} \sim 25^\circ\text{C}$.²⁶ The T_m of the α -synuclein:DMPS system was found to increase from $\sim 25^\circ\text{C}$ before PK treatment to $\sim 41^\circ\text{C}$ after PK-treatment (Figure S3 A), suggesting that the incubation of α -synuclein-DMPS mixtures with PK leads to the virtually complete removal of the protein from the surface of the vesicles. The mechanism of this displacement is likely to be the digestion of the free monomeric α -synuclein, which is highly susceptible to PK digestion due to its intrinsically disordered nature, and the resulting displacement of

the binding equilibrium caused by the decreased lipid-affinity of the proteolytic fragments. Circular dichroism (CD) spectra of α -synuclein-DMPS mixtures before and after addition of PK confirmed that the secondary structure of the protein changed from mainly α -helical to random-coil upon PK treatment (Figure S3 B), reflecting again the digestion of α -synuclein into short, unstructured peptides.

Having established a method to remove the bound α -synuclein *in situ*, we then acquired the SAXS data of the PK treated protein-vesicle mixtures for DLPS and DMPS and found that they closely superimpose with those of intact vesicles before protein addition (Figure 1 A,B). Indeed, the $p(r)$ -distribution profiles of the PK treated α -synuclein:lipid mixtures are typical of large vesicles and the corresponding SAXS data are well-described by the polydisperse three-shell vesicle model (Figure 1 A and B) with structural parameters similar to those of intact vesicles before protein addition (Table 5 and 1). In order to achieve a satisfying fit, the vesicles formed after PK treatment of the α -synuclein:lipid mixtures require a polydisperse distribution of thicknesses of the lipid shell as well as the radius, whereas the initial intact vesicles only required a distribution of radii.

Table 5: Structural parameters refined from the SAXS data of PK treated protein-lipid mixtures and DMPS vesicles shown in Figure 1 using the Three-shell vesicle model. The model was calculated on absolute scale. *Parameter fixed during refinement. - means the parameter was not required to describe that data set.



Parameters	DLPS + α -synuclein + PK	DMPS + α -synuclein + PK	DMPS + PK
Scale	1*	1*	1*
Radius [Å]	197 ± 15	101 ± 10	263 ± 73
σ_{Radius}	0.30 ± 0.04	0.38 ± 0.05	0.32 ± 0.1
v_{lipid} [Å ³]	941 ± 1	1066 ± 3	1060 ± 3
t_{lipid} [Å]	17.7 ± 0.5	18.7 ± 0.5	19.9 ± 0.2
σ_t	0.19 ± 0.05	0.11 ± 0.08	-
Roughness [Å]	3.66 ± 0.36	4.42 ± 0.40	4.41 ± 0.21
Background [cm ⁻¹]	0.0006 ± 0.0004	0.0007 ± 0.0003	0.0002 ± 0.0002
χ^2	4.32	3.21	1.95

The treatment of the vesicles with PK does not in itself affect their SAXS profiles and $p(r)$ distribution profiles (Figure S4). When we refine the three-shell vesicle model against the data collected from DMPS with PK, we obtain very similar results to the pure DMPS vesicles, Table 5. Moreover, the SAXS profile of DMPS vesicles in the presence of PK-

pre-digested α -synuclein, is characterized by an increase of the first minimum (at $q \sim 0.04 \text{ \AA}^{-1}$) compared to the DMPS vesicles data without a shift to higher q (Figure S4). This observation is consistent with conserved vesicles with α -synuclein in a Gaussian random coil conformation partly in solution and partly surface bound but without significant disruptions of the vesicles. From the $p(r)$ -distributions it is evident that the overall vesicle structure is hardly affected by this short peptide-vesicle interaction.

Taken together, these results indicate that the structural changes to small discs induced by the binding of α -synuclein to DLPS and DMPS vesicles can be reverted by removal of the protein. The reformed vesicles have a similar size to that of intact vesicles before α -synuclein binding but with a higher polydispersity compared to the pure vesicle samples.

We further investigated the reversibility of the binding of α -synuclein to DMPS vesicles using temperature-ramp experiments. α -synuclein binding to DMPS vesicles was found to be more favourable when the membrane was in the fluid phase than in the gel phase,²⁶ with the stoichiometry of lipid-binding differing by approximately one order of magnitude between the two phase states of the lipid. Therefore, when DMPS disks saturated with protein are cooled from above to below the melting temperature, $\sim 90\%$ of the protein can be expected to detach and the DMPS lipids to re-organise themselves into vesicles, if the interaction is reversible.

We measured SAXS data of DMPS vesicles in the absence and the presence of α -synuclein at temperatures ranging from $14 \text{ }^\circ\text{C}$ to $48 \text{ }^\circ\text{C}$ (Figure 3 and S5), temperatures at which the DMPS bilayer is in the gel phase and fluid phase, respectively, irrespective if the protein is bound or not.²⁶

The increase of temperature from $14 \text{ }^\circ\text{C}$ to $30 \text{ }^\circ\text{C}$ led to a decrease of the intensity at low- q from ~ 2 to 0.6 cm^{-1} , a decrease in the initial decay of the profiles and a shift of the position of the first intensity minimum to higher- q for the SAXS profile of α -synuclein:DMPS vesicle mixture (Figure 3A). The reduction in forward scattering points towards the break-up of DMPS vesicles into smaller particles that contain a lower number of lipids. Such changes

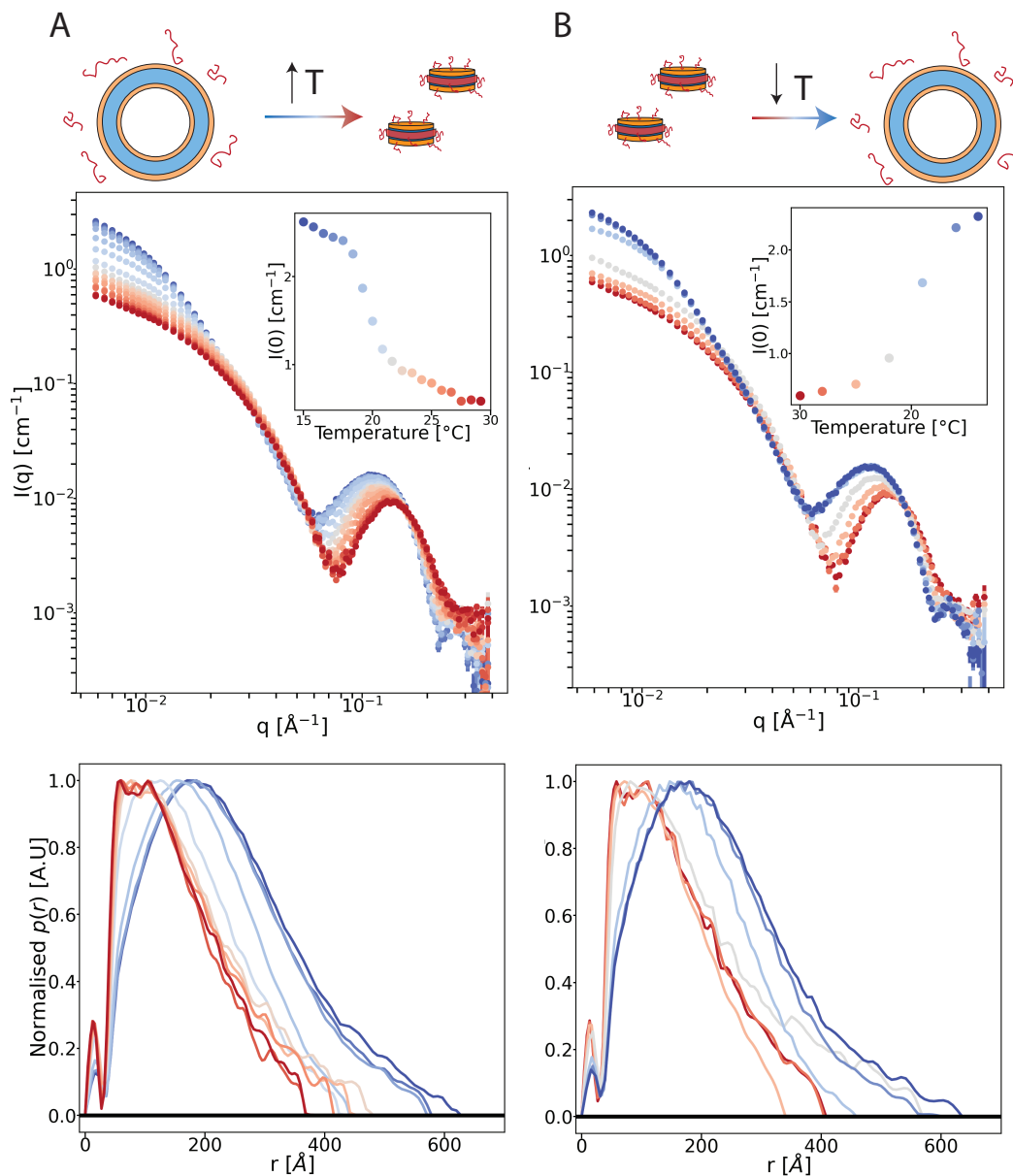


Figure 3: Structural characterisation of the α -synuclein:DMPS system at increasing and decreasing temperature using SAXS. X-ray scattering and normalized $p(r)$ -distribution profiles of (A) 3 mM DMPS in the presence of 100 μM α -synuclein heated from 14 $^{\circ}\text{C}$ to 30 $^{\circ}\text{C}$ and (B) 3 mM DMPS in the presence of 100 μM α -synuclein cooled from 30 $^{\circ}\text{C}$ to 14 $^{\circ}\text{C}$. Insets: the first data point ($q = 0.0048 \text{ \AA}^{-1}$) of each SAXS profile as a function of temperature in order to highlight the transition temperature of the system at $\sim 20 \text{ }^{\circ}\text{C}$.

were not observed for the pure DMPS vesicles when the temperature was increased from 14 $^{\circ}\text{C}$ to 49 $^{\circ}\text{C}$ (Figure S5). The scattering profiles of the first five temperatures (14 $^{\circ}\text{C}$ to 18 $^{\circ}\text{C}$) of α -synuclein:DMPS vesicle mixture lie approximately on top of each other and their $p(r)$ -

distribution profiles are indicative of spherical particles with a D_{max} of at least 600 Å (Figure 3A). Between 19 °C and 20 °C, however, a clear transition can be observed, corresponding to the melting of α -synuclein bound DMPS bilayers. The temperature-dependence of the profiles levels off again around 25°C suggesting the DMPS: α -synuclein co-structures may have reached a new (meta-)stable structural state. At these temperatures (T above 25°C), $p(r)$ -distribution profiles resemble that of disk-like particles³³ with a prominent flat maximum at $r = 50$ to 150 Å and a tail at long distances (Figure 3A).

Figure 3B shows that the structural changes that DMPS vesicles undergo upon binding of α -synuclein can be reversed by cooling the system back down to 14 °C. As the temperature was decreased from 30 °C to 14 °C, we observed the transition of α -synuclein-bound DMPS bilayer around 19°C and the shape and intensity of the SAXS profile after cooling was restored to that before cooling. The $p(r)$ -distribution profiles of the DMPS: α -synuclein co-structures below the melting temperature for the heating (Figure 3A) and cooling (Figure 3B) measurements are very similar, suggesting that the structural changes of the vesicles upon α -synuclein binding can be reversed upon detachment/removal of the protein induced by cooling.

We again attempted to refine structural models against data collected at various temperatures (Figure 4). Since scattering contribution from α -synuclein must now be included throughout the series of measurements, we expand the three-shell vesicle model described earlier into a four-shell vesicle model (Figure S9). The four-shell vesicle model assumes some protein becomes embedded in the outer leaflet headgroups and tailgroups. From inside to outside the shells of the four-shell vesicle model represent lipid headgroups, lipid tailgroups, lipid tailgroups with some contribution from α -synuclein, and lipid headgroups with some contribution from α -synuclein (Figure S9). Gaussian random coils are attached to the outside of the vesicle following the procedure detailed by Arleth *et al.*,⁴¹ to describe the hydrophilic domain of α -synuclein which does not become embedded in the lipids. Furthermore, the scattering intensity arising from α -synuclein free in solution is also modelled as Gaussian

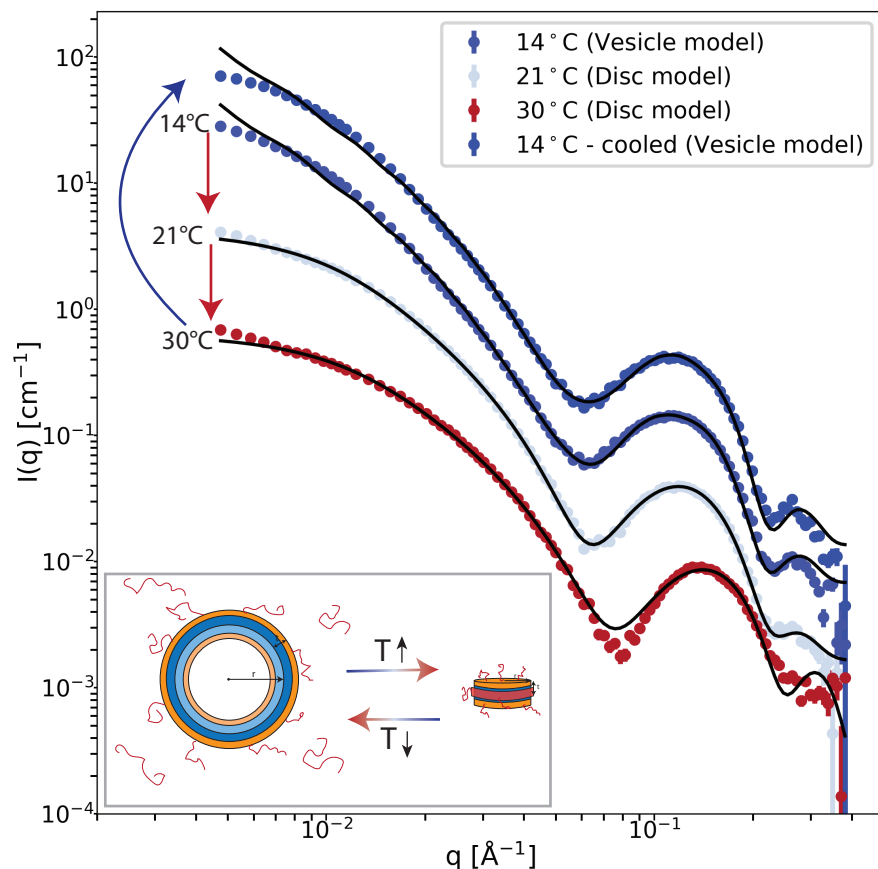


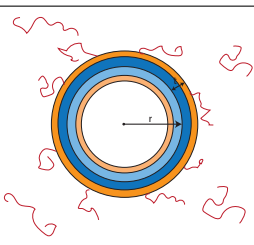
Figure 4: Structural modelling of the SAXS data investigating the reversible structural reorganisation of DMPS: α -synuclein from vesicles to discs with increasing temperature and hence binding of α -synuclein. For ease of viewing, the data are scaled by 2^n where n is the profile number, so the bottom scattering profile (30°C) has $n = 0$ and remains on absolute scale, and the topmost profile has $n = 3$. The refined structural parameters are listed in Tables 6 and 7.

random coils. This 'Four-shell vesicle with random coils' model is illustrated in Figure 4 and described in greater detail in the SI.

For both the heating and cooling measurements, the X-ray scattering profiles of the DMPS: α -synuclein mixture at 14°C can be described with the 'Four-shell vesicle with Gaussian random coils' model (Figure 4). The refined parameters, given in Table 6, are almost identical for the heating and cooling experiments confirming that the initial state of the vesicles is fully restored upon cooling-induced dissociation of α -synuclein. Again the $R_{g\ \alpha\text{-syn}}$ of the random coils protruding from the surface of the vesicle was poorly resolved during the

refinement and hence fixed to 18 Å, as above. We do however note that the radius of gyration R_g for the free unbound α -synuclein of 33 ± 4 Å is in very close agreement with Kohn’s estimation of 37 Å for 140 residues. We see that around 12% of the α -synuclein is bound to the lipids, as expected from the previously determined stoichiometry at this temperature (i.e. 300 DMPS lipids per α -synuclein monomer).²⁶ We observe an increase in the thickness of the lipid leaflets compared to lipid vesicles without α -synuclein. Here we choose to fix the roughness at 5 Å to keep the 2nd maximum at $q = 0.3 \text{ \AA}^{-1}$ visible in the model, which would be smeared into the background if the roughness was > 5 Å. The model overshoots the data at low- q , which we believe could be due to an intra-particle structure factor effect but note that this is difficult to model with polydisperse systems such as this.

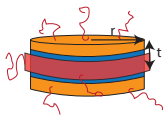
Table 6: Structural parameters refined from the data in Figure 4 using the Four-shell vesicle with Gaussian random coils model. The model was calculated on absolute scale. *Parameters fixed during refinement.

	Parameter	14 °C	14 °C after cooling
	Scale	1*	1*
	Fraction of α -synuclein bound	0.12 ± 0.008	0.13 ± 0.007
	$R_{g, \text{ bound } \alpha\text{-syn}}$ [Å]	18*	18*
	Radius [Å]	363 ± 16	363 ± 14
	σ_{Radius}	0.29 ± 0.004	0.30 ± 0.003
	v_{lipid} [Å ³]	989 ± 4	989 ± 3
	r_{lipid} [Å]	23.4 ± 0.3	23.2 ± 0.3
	$R_{g, \text{ free } \alpha\text{-syn}}$ [Å]	32.8 ± 4.3	33.7 ± 4.0
	Roughness [Å]	5*	5*
	Background [cm ⁻¹]	0.0007 ± 0.0002	0.0006 ± 0.0002
	χ^2	60.6	100

For temperatures above 21°C, i.e. just above the transition, the low- q slope of X-ray scattering profiles of DMPS: α -synuclein mixtures could not be described by a vesicle model. Instead, the ‘Disc with Gaussian random coils’ model, introduced above and described in the SI, achieves a more convincing fit (Figure 4). Since much more of the protein binds to the lipid particles above the T_m , we assume the scattering contribution from the free α -synuclein to be negligible in this high binding regime. At 30 °C, we assume that 100 % of α -synuclein is bound to the lipid bilayer and therefore fix the molar ratio of DMPS: α -synuclein to 30:1 in line with the experimental concentrations. At 21 °C, we are able to refine a ratio of lipid

to bound- α -synuclein of 68 ± 37 , corresponding with 45% of α -synuclein, although with a relatively large uncertainty. The model fit results show polydisperse discs with an average radius and bilayer thickness of 153 Å and 50 Å, respectively at 21 °C, which are reduced to 126 Å and 47 Å at 30 °C (Table 7).

Table 7: Structural parameters refined from the data in Figure 4 using the Disc with Gaussian random coils model. *Parameters fixed during refinement.



Parameter	21°C	30°C
Scale	1*	1*
L/P	67.5 ± 36.9	30*
w_{Belt} [Å]	12*	12*
$R_{\text{g}, \alpha\text{-syn}}$ [Å]	18*	18*
Radius [Å]	153 ± 19	126 ± 21
σ_{Radius}	0.33 ± 0.02	0.39 ± 0.02
v_{lipid} [Å ³]	954 ± 36	880 ± 81
$v_{\alpha\text{-syn}}$ [Å ³]	19600 ± 890	21300 ± 530
t_{lipid} [Å]	24.9 ± 1.2	23.6 ± 0.5
Roughness [Å]	5.21 ± 1.10	1.78 ± 1.29
Background [cm ⁻¹]	0.0005 ± 0.0004	0.0002 ± 0.0005
χ^2	2.36	7.05

Taken together, these results show that the structural changes from vesicles to smaller discs that DMPS and DLPS undergo upon the initial binding of α -synuclein can be largely reversed, either by degradation-induced protein displacement (demonstrated for DMPS and DLPS) or by temperature-induced partial displacement of the protein from the membrane (demonstrated for DMPS).

α -synuclein-lipid structures elongate during the process of amyloid formation

Finally, we used Small Angle Neutron Scattering (SANS) measurements under protein and lipid contrast-matching conditions to study the individual structural contribution of the protein and lipid molecules to the process of amyloid fibril formation. Indeed, this technique allows the acquisition of the neutron scattering intensity of a mixture containing lipid vesicles and α -synuclein under various D₂O:H₂O contents to match out either the signal of the protein or that of the lipid vesicles. Our SANS measurements of deuterated α -synuclein (d- α -synuclein) and DMPS or DLPS vesicles in D₂O concentrations ranging from 0 to 100%

show that the forward scattering of the protein and the lipids are matched out in the presence of 100% and 18% D₂O, respectively (Figure S6).

We then measured the neutron scattering profiles of d- α -synuclein-DMPS mixtures under protein contrast-matching conditions at temperatures ranging from 14 to 31 °C (upwards and downwards, as described above) and their analyses using model fits confirmed the reversible break-up of lipid vesicles into small structures upon the binding of the protein (Figure S13). We also performed a titration experiment, where we added the α -synuclein in small portions and measured the dependence of the scattering function under protein-matched conditions as a function of α -synuclein concentration (Figure S12). We found that the decrease in scattering intensity at low q -values was non linear in protein concentration. The addition of small quantities of α -synuclein led to a stronger than proportional decrease of scattering intensity. This finding suggests a lower degree of binding cooperativity than previously reported for another α -synuclein-lipid system (see discussion in the supplementary results).

Having established the reversibility of the rapid structural re-arrangement of the lipid vesicles upon α -synuclein binding using SAXS (Figures 1 - 4) and SANS (Figures S13, S15) measurements, as well as temperature-dependent dynamic light scattering (DLS) experiments (Figure S16 and S17), we investigate in more detail the subsequent aggregation process that occurs on a much slower time scale of hours to days.^{22,26} Due to the better compatibility of the fast DLPS-induced aggregation of α -synuclein (compared to DMPS) with the time scale of SANS measurements, we used exclusively DLPS in these kinetic experiments. We prepared several samples under identical conditions, except for the ratios of D₂O to H₂O (100% D₂O (Figure 5A) and 18% D₂O (Figure 5B)) and the absence or presence of the fluorescent dye Thioflavin-T (ThT), which reports on the formation of amyloid fibrils. The sample with ThT allowed us to follow the formation of fibrils in real time by monitoring the increase in fluorescence intensity over time in a plate reader (Figure 5C, black curve). While the binding of α -synuclein to lipid vesicles initially leads to a strong decrease of the scattering function at low q values under protein matching conditions (Figure S12 B),

the intensity increases at low q as a consequence of the slow aggregation process (Figure 5A). Simultaneously, the scattering intensity decreases at higher q values, with an isosbestic point at $\sim 0.07 \text{ \AA}^{-1}$. Between 14 and 20 hours, the scattering profiles lie on top of each other suggesting the particles have evolved to a stable state. Under lipid-matching conditions, on the other hand, the scattering intensity at low q values increases rapidly upon binding of α -synuclein to the lipid vesicles and continues to increase during the slower aggregation process (Figure 5 B). Both the change in lipid and protein scattering signal occur on a time scale very similar to that of the accompanying ThT experiments (Figure 5C). These results show that the aggregation of α -synuclein is accompanied by a large scale rearrangement of the lipids, strongly supporting the hypothesis that lipid molecules are incorporated into the protein-rich aggregates.²⁴

We were able to model the kinetic neutron scattering profiles in 100% D₂O as the emergence of cylinders with increasing dimensions, where the fitting parameters were the radius R , length L and scale. The cylinders were assigned a "bulk" scattering length density corresponding with a molar ratio of DLPS:d- α -synuclein 10:1 in line with the experimental conditions. A free scale parameter was required to correct the scattering length density of the lipid particle as more d- α -synuclein becomes incorporated and decreases the overall contrast, as well as ambiguity in calculating the number density of scatterers. At $t = 2$ min, already the data indicate rods with $R=18 \text{ \AA}$ and $L=210 \text{ \AA}$. Between 1 and 4 hours, there is a significant upturn at low- q in the data which cannot be captured by the single-state cylindrical form factor. We hypothesize that this upturn present in the data collected between 2 min and 4 hours indicates the presence of one or more populations of much larger structures; potentially a population of fibril-like structures which have matured on a shorter time-scale. Therefore the cylindrical model fits to these data capture the smaller population of scatterers. From 6 hours onward, the upturn is no longer present and the model can be employed to describe the entire scattering profiles. The refined parameters indicate long cylinders of at least 700 \AA . The data at low- q do not contain a Guinier region or any initial plateau and

hence the maximum dimension of the cylinders is outside the size range accessible by the experimental setup. For this reason, when refining the length of these cylinders we obtain a very large uncertainty of around 50%. The associated fit parameters can be found in Table 8.

The data collected in 18% D₂O displays other types of features and reflects the complicated underlying structure of fibrils of α -synuclein. There is a drop in forward scattering between 5 minutes and 1 hour (Figure S12 B) indicating there is some initial transformation in the arrangement of α -synuclein within the lipid co-structure before the fibril formation process begins. The scattering profiles collected after 1, 2, 4 and 6 hours fall closely on top of each other showing the protein structure remains largely unchanged and there is a lag in the aggregation process. The scattering profiles at these early time points contain a strong Guinier range and do not indicate the presence of a sub-population of very large particles, which are obvious in the data collected in 100% D₂O (Figure 5), suggesting these large intermediate structures must be composed mainly of lipids. Between 6 and 20 hours there is a systematic increase in the forward scattering of the data indicating that the volume of the α -synuclein-associated particles is growing. After 18 hours the Guinier range becomes completely diminished indicating the protein also forms structures which are outside the size range accessible by the experimental setup.

We first modelled these data with the form factor for cylinders which was only sufficient at low- q . The data points above $q = 0.02 \text{ \AA}^{-1}$ are much more indicative of a flexible structure, which can be explained as the C-terminus of α -synuclein which is not likely to become part of the fibril core. We therefore use an analytical model for cylinders decorated with Gaussian random coils to represent the fibril core and disordered domains. The cylinder is given the scattering length density corresponding with 10:1 DLPS:d- α -synuclein and therefore has a reduced contribution compared with the coils. The model fits the data series well (Figure S12 C) but due to low statistics arising from the H₂O in the sample buffer, the refined parameters are highly correlated and poorly defined (Table S4). The data can be modeled on absolute

scale without the use of a free scale parameter, potentially due to the fact that the signal is partly made up of coils of α -synuclein whose contrast is unaffected by the presence of lipids. Minor corrections to the absolute scaling may be absorbed by the other free parameters. The refined parameters at 5 minutes and 1 hour potentially reflect the initial decrease in scattering intensity as the length drops from 231 to 175 Å. The model captures a growth of the cylinders that is less extreme than what is seen in the 100% D₂O protein-matching conditions. The cylinders appear to grow in length from 170 to 300 Å while maintaining a radius close to 20 Å. The R_g of the protruding α -synuclein, between 33 and 40 Å, is larger than expected for the 44 hydrophobic amino acids in the C-terminus but could reflect larger or extended disordered regions of the fibril structure. However, the systematic growth in the R_g of the protruding α -synuclein is unexpected and this parameter may be inadvertently reflecting a thickness increase of the fibril core.

Table 8: Structural parameters refined from the SANS data in Figure 5 D using a simple cylinder model.

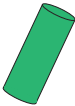
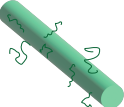
		Scale	Radius [Å]	Length [Å]	Background [cm ⁻¹]	χ^2
	2 mins	3.92 ± 0.43	18.1 ± 1.2	209 ± 23	-	1.43
	1 h	4.00 ± 0.46	18.0 ± 1.3	186 ± 20	-	5.43
	2 h	3.81 ± 0.43	18.3 ± 1.3	186 ± 20	-	7.41
	4 h	3.44 ± 0.35	19.0 ± 1.2	255 ± 34	-	8.71
	6 h	1.45 ± 0.37	28.6 ± 3.2	705 ± 476	0.023 ± 0.008	2.45
	8 h	1.33 ± 0.21	32.2 ± 2.2	645 ± 347	0.025 ± 0.006	1.69
	10 h	1.22 ± 0.14	36.5 ± 1.7	705 ± 395	0.026 ± 0.005	2.96
	12 h	1.22 ± 0.12	38.3 ± 1.5	675 ± 334	0.025 ± 0.004	4.80
	14 h	1.23 ± 0.11	39.8 ± 1.4	690 ± 336	0.024 ± 0.004	6.68
	16 h	1.23 ± 0.10	40.8 ± 1.4	686 ± 319	0.024 ± 0.004	7.37
	18 h	1.24 ± 0.10	40.7 ± 1.4	677 ± 309	0.024 ± 0.004	8.58
	20 h	1.23 ± 0.11	40.6 ± 1.4	714 ± 353	0.023 ± 0.004	9.38

Table 9: Structural parameters refined from the SANS data in Figure 5 E using a cylinder decorated with Gaussian random coils. *Parameter fixed during refinement

		Scale	Radius [Å]	Length [Å]	R_g [Å]	Background [cm ⁻¹]	χ^2
	5 mins	1*	19.7 ± 5.56	231 ± 160	37.5 ± 23.1	0.050 ± 0.010	1.22
	1 h	1*	19.4 ± 13.3	175 ± 240	33.9 ± 42.0	0.052 ± 0.013	1.22
	2 h	1*	19.5 ± 14	172 ± 248	33.3 ± 43.6	0.051 ± 0.013	1.06
	4 h	1*	19.5 ± 14	175 ± 233	33.2 ± 40.0	0.051 ± 0.012	1.17
	6 h	1*	19.8 ± 9.9	188 ± 196	33.8 ± 32.2	0.052 ± 0.011	1.06
	8 h	1*	20.9 ± 9.4	189 ± 168	38.2 ± 30.8	0.053 ± 0.013	0.85
	10 h	1*	20.7 ± 6.3	221 ± 151	36.5 ± 22.5	0.054 ± 0.010	0.94
	12 h	1*	20.7 ± 4.7	245 ± 135	36.3 ± 17.5	0.055 ± 0.010	0.98
	14 h	1*	21.4 ± 4.6	253 ± 132	37.9 ± 17.1	0.052 ± 0.010	1.31
	16 h	1*	21.9 ± 3.9	274 ± 127	39.0 ± 15.0	0.052 ± 0.010	1.36
	18 h	1*	22.4 ± 3.5	288 ± 122	39.1 ± 13.3	0.052 ± 0.010	1.29
	20 h	1*	23.3 ± 3.6	297 ± 122	41.9 ± 13.7	0.051 ± 0.010	1.61

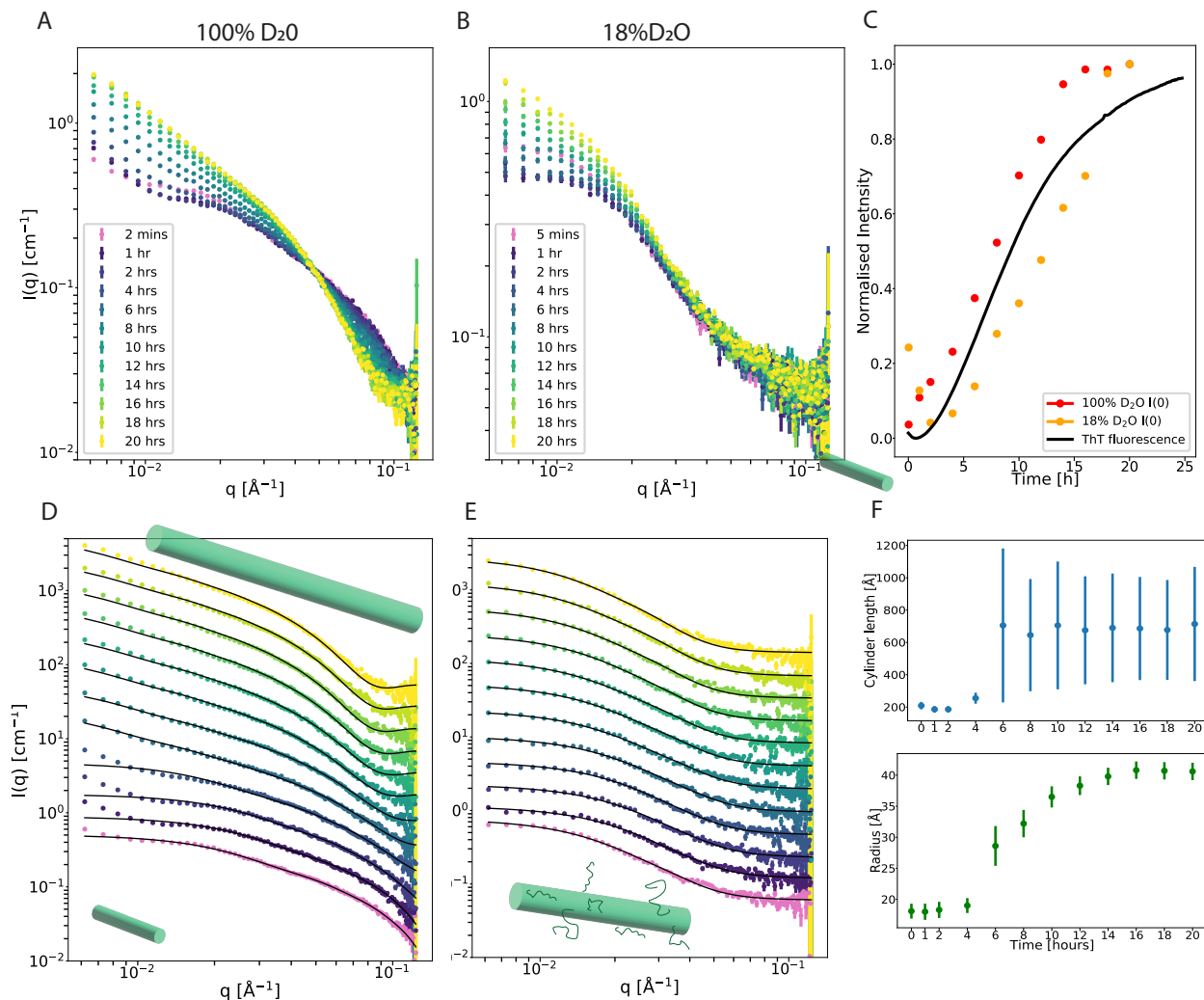


Figure 5: The morphology of DLPS vesicles and α -synuclein changes within the same time scale as amyloid formation, as monitored by Thioflavin-T fluorescence. Neutron scattering function of the reaction mixture 2 mM DLPS + 200 μ M α -synuclein measured at 30 °C over time in buffer conditions corresponding to the contrast matching of the protein, 100% D₂O (A) or the vesicles, 18% D₂O (B). (C) Normalized change in the ThT fluorescence and the forward scattering of the reaction mixture under both contrast conditions. (D) Cylindrical model fits refined against each scattering profile collected under the contrast matching of the protein, 100% D₂O. (E) Model fits refined against each scattering profile collected under the contrast matching of the lipid, 18% D₂O. The model depicts a cylinder decorated with Gaussian random coils. For ease of viewing, the data are scaled by 2^n where n is the profile number, so the bottom scattering profile (pink, 2 min) has $n = 0$ and remains on absolute scale and the top scattering profile (yellow, 20 hours) has $n = 11$. (F) Refined fit parameters from the data fits in (C), cylindrical length and radius as a function of time, indicating significant growth in both dimensions, particularly in the length dimension.

All together, our SANS measurement of the α -synuclein-DLPS mixtures show that both the lipid and protein molecules undergo structural re-arrangements characteristics of cylinder growth during the same time scale as that of the formation of amyloid fibrils, demonstrating their co-assemblies.

Discussion

Protein-lipid interactions have long been recognized as a key process involved in the initiation and / or modulation of the formation of amyloid fibrils by peptides and proteins associated with neurodegeneration, such as α -synuclein, amyloid β or IAPP.^{22,47-49} These proteins have high affinities towards certain types of lipid membranes, depending on the solution conditions and the physical and chemical properties of the lipids, such as charge, length of the acyl chain, degree of unsaturation and phase state of the lipid bilayer.²⁶ These interactions, as well as their consequences for amyloid fibril formation, have been studied in detail. The relative concentrations of lipids and peptides have emerged as a key control parameter that defines in many cases whether lipids accelerate or slow down amyloid fibril formation.^{22,47,49} Detectable (by ThT fluorescence) amounts of amyloid fibrils usually only form if there is a significant excess of monomeric peptide in solution over the amount that saturates the lipid membranes,²² even though it has also been demonstrated by microscopy that fibrils can form on the membrane at exceedingly low protein concentrations.^{50,51} The interactions with lipid membranes are often part of the physiological functions of the amyloidogenic peptide, as is in particular also the case for α -synuclein.^{7,52} A finely tuned balance appears to exist between benign and detrimental lipid-protein interactions and it has been proposed that the onset of pathology and disease may be caused if the system gets out of balance, e.g. due to age-related chemical modifications of protein and lipids, as well as changes in protein concentration.⁴⁷ The mechanism by which lipid-binding can facilitate and induce amyloid fibril formation is still not fully understood for any such system. In the simplest view, the binding

of the protein to the lipid bilayer increases the local protein concentration and/or changes protein conformation, both of which can favour aggregation. However, in the framework of this simple mechanism, the lipid bilayer acts as a mere catalyst and, assuming that the aggregates can detach from the bilayer, a small amount of lipid vesicles should be able to induce the amyloid fibril formation of a large excess of protein. However, for α -synuclein, this is not observed. On the contrary, the quantity of aggregates formed is proportional to the initial concentration of lipids, and if a small amount of lipid vesicles is added at the beginning, the aggregation reaction stops before all the monomeric protein has been converted into aggregates in the absence of secondary processes.^{22,26} This behaviour can only be rationalized if it is assumed that the lipids are a reagent and are being consumed from the membrane as the amyloid aggregates form.

The results of our extensive scattering measurements on α -synuclein-lipid systems show that the binding of the protein to lipid vesicles leads to a major structural re-arrangement into small particles, that is followed by the incorporation of lipid molecules into the aggregates, and strongly support this model. The main contribution and novelty of the present study is the ability to clearly distinguish between the very rapid (ms time scale) structural change induced by the binding of the protein to the lipid vesicles and the structural changes associated with the amyloid formation that occur on a time scale of hours. We were unable to resolve the kinetics of initial binding by stopped-flow SAXS; suggesting that the binding reaction occurs in a few ms, and is essentially diffusion-limited. DLS, SAXS, and SANS experiments show that at temperatures below the melting transition, the protein coats the vesicles, which remain largely intact. At temperatures above the melting transition (ca. 21-23°C for DMPS), this interaction immediately leads to a major structural change of the lipid vesicles, i.e. a break-up into smaller particles. Interestingly, this break-up is largely reversible when the protein is removed, either by cooling down or by enzymatic digestion of the protein. In the SAXS experiments, these smaller particles could be well-described by a model for disc-like particles, reminiscent of α -synuclein-stabilized nanodiscs,¹⁷ whereas the

SANS data were more consistent with the formation of rod-like structures. This apparent discrepancy can be explained by the fact that these structures are probably very similar in energy, and mixtures of different shapes have indeed previously been observed in a very similar system.⁵³ Whether a given mixture tends more towards the formation of discs or rods presumably depends on subtle differences, such as for example differences in the solvent (purely hydrogenated water for SAXS, partly or fully deuterated water in the case of SANS). However, both techniques agree in that the resulting structures have significantly lower volume and hence scattering intensity, compared to the original vesicles. The lipid systems that were characterized in detail in this study (DLPS and DMPS), and which were demonstrated to undergo a strong structural disruption upon interaction with α -synuclein, are both known to efficiently induce amyloid fibril formation.^{22,26} In the case of DLPS, the SANS measurements show that the lipids are being incorporated into the fibrils, which is in agreement with a range of previous studies.^{23-25,54-56} It is interesting to speculate that there is a close connection between the ability of the protein to disrupt the lipid vesicles and the lipids to induce amyloid fibril formation. Such a hypothesis is supported by the observation that lipids that form vesicles that are not disrupted (e.g. POPG) by α -synuclein binding are also not efficiently inducing amyloid fibril formation.¹⁰ Therefore the simple adsorption onto the lipid bilayer, despite increasing the local concentration of α -synuclein on the vesicle surface, does not seem to be the main cause of the observed acceleration of amyloid fibril formation upon lipid binding. Rather, the formation of intricately mixed protein-lipid nanostructures, discs or rods, in which the lipid molecules or membranes might mediate favourable protein-protein interactions, seem to be the most efficient inducer of amyloid fibril formation. This model provides a mechanistic framework that can be used to analyse the effect of lipid modifications that are suspected to favour deleterious protein-protein interactions leading to amyloid fibril formation.

Conclusion

In conclusion, we have used a combination of time resolved small angle scattering measurements (SAXS and SANS), dynamic light scattering and differential scanning calorimetry in order to investigate the reversibility and structural consequences of the binding of α -synuclein to negatively charged lipid vesicles (DMPS and DLPS). We find that the initial binding of the protein to the lipid vesicles is extremely rapid (faster than 1 ms), easily reversible and leads to a major structural transition and break-up of intact vesicles into significantly smaller disc- and rod-shaped lipid-protein co-assemblies. The resulting subsequent formation of fibrillar aggregates of α -synuclein, leads to yet another substantial structural changes in the lipids that occur on the same time scale as that of the protein aggregation and hence confirms that lipid-protein co-aggregates are formed.

Experimental methods

Protein and lipid samples

Unlabelled α -synuclein was purified as described previously.²² Matchout-deuterated human α -synuclein was produced in the Deuteration Laboratory of the Institut Laue-Langevin (ILL D-Lab, Grenoble, France). To obtain d- α -synuclein, a transposition reaction was first carried out on the original plasmid in order to modify the resistance selection marker from ampicillin to kanamycin. The Tn5 transposon insertion kit (EZ-Tn5™ <KAN-2> Insertion Kit) from Epicentre[®] Biotechnologies/Illumina[®] was used for this transposition reaction. New kanamycin-resistant plasmid containing cDNA coding for human α -synuclein was transformed into One Shot™ BL21(DE3) E. coli cells (Invitrogen). Deuterated α -synuclein was over-expressed in E.coli strain BL21(DE3) adapted to growth in deuterated minimal medium.⁵⁷ A 1.7 L (final volume) deuterated high cell-density fed-batch fermenter culture was carried out at 30°C. Feeding with glycerol was started at an OD₆₀₀ value of about 4.2.

Expression of d- α -synuclein was induced at an OD₆₀₀ of 19 by addition of IPTG (1mM final concentration). Cells were harvested at an OD₆₀₀ of 23 yielding 74 g wet weight of deuterated cell paste. Lipid vesicles were prepared via sonication as described previously .²²

Circular Dichroism (CD) spectroscopy

CD samples were prepared by incubating 267 μ M α -synuclein in the presence of 8 mM DMPS in 20 mM sodium phosphate buffer (pH 6.5). Far-UV CD spectra were recorded using a JASCO J-810 spectropolarimeter equipped with a Peltier thermally controlled cuvette holder at 30°C. The spectra were measured before and after incubation of the sample with 15.7 μ M proteinase-K for 1 hours. The samples were diluted 10 times before measurement.

Differential Scanning Calorimetry

The DSC samples were prepared by incubating 0.86 mM DMPS in the absence or presence of 28.6 μ M α -synuclein in 20mM sodium phosphate buffer pH 6.5. DSC thermograms of these samples untreated or treated with 1.7 μ M proteinase-K for 1 h at 20 °C were acquired using a Microcal VP-DSC calorimeter (Malvern Instruments) with a scanning rate of 1°C.min⁻¹ from 5 to 65°C. Protein and lipid samples were degassed for 20 min at room temperature before mixing and acquisition of the DSC thermograms. The DSC thermograms reported in this article were corrected by subtracting the thermogram of the phosphate buffer and normalized with respect to the lipid concentration.

Small Angle X-ray Scattering

Measurements at ESRF in Grenoble

SAXS experiments were performed at the beamline ID02 at ESRF, Grenoble. SAXS signals were measured at a distance of 2 m. For temperature series, standard temperature-controlled capillary holder at ID02 (capillary diameter 1.5 mm) was used. A fresh solution spot was

used for each temperature to avoid effects of radiation damage. 3 mM DMPS was incubated in the absence or presence of 50 or 100 μM α -synuclein in phosphate buffer pH 6.5 at temperatures ranging from 15 to 65°C. For kinetic series with rapid mixing, a commercial stopped-flow setup (Biologic, SFM 400) adapted for use at ID02 with a special X-ray head with a measurement capillary (1.5 mm diameter) was used.⁵⁸ The dead time was found to range between 2-3 ms. The samples were prepared by mixing DMPS solution with either buffer or α -synuclein solutions to reach the final concentrations specified in the paper. Effects of radiation damage was checked beforehand in static samples, and the acquisition times were adapted accordingly. The modelling/fitting of the resulting SAXS data are described in details in the Supplementary Information.

Measurements with the laboratory X-ray source

SAXS measurements were performed in static capillaries mounted on a SAXSLAB Ganesha 300XL equipped with a temperature regulator Julabo CF41 water bath. 8 mM DMPS was incubated in the absence or presence of 270 μM α -synuclein in phosphate buffer pH 6.5 and the SAXS function was recorded before and after proteinase-K treatment. The sample was and the SAXS function was measured at a q range of 0.003-0.73 \AA .

Small Angle Neutron Scattering

SANS measurements were performed on D22 instrument of Institut Laue Langevin. The samples were in a 1 mm thick suprasil quartz cuvette (Hellma QS 100-1-40), mounted on a 22-position sample rack temperature-regulated by two water baths, enabling a rapid switching between 20, 30 and 45°C. 8 mM DMPS was incubated in the absence or presence of 270 μM α -synuclein in 20mM phosphate buffer pH 6.5. For static measurements, the SANS function was recorded at a q range of 0.006-0.635 \AA using two collimation:sample-detector distance sets: one for small angles (11.2m:11.2m) and one for large angles (1.4m:2m). Kinetics measurements were only performed at small angle configuration. The collimation was

rectangular of 40 mm width and 55 mm height, the sample aperture was of 7mm width and 10 mm height and the wavelength was 6 Å +/- 10%. Data were reduced using Grasp software, including blocked beam and empty cell background subtraction, sample thickness normalisation, and absolute intensity scaling using direct beam intensity measurement. Data are permanently curated at ILL.^{59,60}

Aggregation measurements

Samples were prepared by mixing α -synuclein, DLPS or DMPS solutions at the protein-to-lipid ratios indicated in the manuscript together with Th-T (50 μ M) in 20 mM sodium phosphate buffer (pH 6.5). The kinetics of amyloid formation were measured at 30^{circ}C under quiescent conditions in Corning 96 well plates with half-area (black/clear bottom polystyrene) non-binding surfaces using a BMG plate reader.

Dynamic light scattering

The temperature-ramp experiments were performed with a Prometheus Panta (Nanotemper, Munich), which is a microcapillary-based instrument that combines differential scanning fluorimetry (DSF) and dynamic light scattering (DLS) measurements. In the present study we used solely the DLS functionality. The samples were prepared with protein and lipid solutions and buffer that was cooled to below the starting temperature of the temperature ramp (15°C). We measured pure lipids (DMPS and DLPS) at 1 mM, as well as in the presence of 9.5 and 95 μ M α -synuclein. The temperature was varied from 15-35°C and back to 15°C, at two different scan rates (0.5 and 5°C/min) and we plot the cumulant radius from the DLS measurements, as well as the absolute light scattering intensity, as a function of temperature.

Acknowledgement

The authors thanks the Novo Nordisk Foundation (NNFSA170028392, AKB), the Lundbeck Foundation (R314-2018–3493 (CG, FRM) and R155-2015–2666 (AB)) and the European Union’s Horizon 2020 research and innovation programme under the Marie Skłodowska-Curie grant agreement No. 706551 (CG) for support. We acknowledge the European Synchrotron Radiation Facility (ESRF) for provision of synchrotron radiation facilities and we would like to thank Rajeev Dattani for assistance and support in using beamline ID02. We acknowledge the Institut Laue Langevin (ILL) for access to the Deuteration Laboratory (D-Lab) and for providing two beamtimes at the SANS instrument D22.^{59,60}

Supporting Information Available

The following files are available free of charge.

- Figure S1: Additional repeats of the stopped-flow SAXS measurements of the binding between DMPS or DLPS vesicles and α -synuclein
- Figure S2: Model fits to the SF-SAXS data at 0, 1 and 21 ms for DLPS or DMPS mixed with α -synuclein
- Figure S3: Differential scanning calorimetry and circular dichroism measurements of the α -synuclein:DMPS system before and after proteinase-K treatment
- Figure S4: X-ray scattering control experiments for the PK-treatment of the DMPS: α -synuclein system
- Figure S5: X-ray scattering profiles of DMPS vesicles at different temperatures
- Figure S6: Determination of the contrast match points of the protein and DMPS and DLPS vesicles at different temperatures

- Supplementary Methods - Models for the analysis of the SAS data

Figure S7: Schematic of the three-shell vesicle model

Figure S8: Schematic of the disc model with Gaussian random coils

Figure S9: Schematic of the four-shell vesicle model with Gaussian random coils decorating the outer shell

Figure S10: Schematic of the core-shell ribbon model

Figure S11: Schematic of the core-shell cylinder decorated with random coils

- Supplementary Results - Analyses of the SANS and DLS data

Figure S12: Structural characterisation of DMPS and DLPS vesicles upon binding of α -synuclein using SANS

Figure S13: Structural characterisation of the α -synuclein:DMPS system at increasing temperature using SANS

Figure S14: Neutron scattering function of DMPS vesicles measured under protein (100% D₂O) contrast matching conditions at increasing temperature

Figure S15: Structural modelling of the SANS data showing the evolution in the phospholipid particles with increasing temperature and hence binding of α -synuclein

Figure S16: Temperature-dependent DLS experiments of DLPS vesicles in the absence or presence of different concentrations of α -synuclein

Figure S17: Temperature-dependent DLS experiments of DMPS vesicles in the absence or presence of different concentrations of α -synuclein

References

- (1) Dobson, C. M. Protein folding and misfolding. *Nature* **2003**, *426*, 884–890.

- (2) Spillantini, M. G.; Schmidt, M. L.; Lee, V. M.; Trojanowski, J. Q.; Jakes, R.; Goedert, M. Alpha-synuclein in Lewy bodies. *Nature* **1997**, *388*, 839–840.
- (3) Mahul-Mellier, A.-L.; Burtscher, J.; Maharjan, N.; Weerens, L.; Croisier, M.; Kutler, F.; Leleu, M.; Knott, G. W.; Lashuel, H. A. The process of Lewy body formation, rather than simply α -synuclein fibrillization, is one of the major drivers of neurodegeneration. *Proceedings of the National Academy of Sciences* **2020**, *117*, 4971–4982.
- (4) Burré, J.; Vivona, S.; Diao, J.; Sharma, M.; Brunger, A. T.; Südhof, T. C. Properties of native brain α -synuclein. *Nature* **2013**, *498*, E4–6; discussion E6–7.
- (5) Theillet, F.-X.; Binolfi, A.; Bekei, B.; Martorana, A.; Rose, H. M.; Stuver, M.; Verzini, S.; Lorenz, D.; van Rossum, M.; Goldfarb, D.; Selenko, P. Structural disorder of monomeric α -synuclein persists in mammalian cells. *Nature* **2016**, *530*, 45–50.
- (6) Fusco, G.; Simone, A. D.; Gopinath, T.; Vostrikov, V.; Vendruscolo, M.; Dobson, C. M.; Veglia, G. Direct observation of the three regions in α -synuclein that determine its membrane-bound behaviour. *Nat Commun* **2014**, *5*, 3827.
- (7) Bendor, J.; Logan, T.; Edwards, R. H. The Function of α -Synuclein. *Neuron* **2013**, *79*, 1044–1066.
- (8) He-Jin Lee, C. C.; Lee, S.-J. Membrane-bound α -Synuclein Has a High Aggregation Propensity and the Ability to Seed the Aggregation of the Cytosolic Form. *J Biol Chem* **2002**, *277*, 671–678.
- (9) Zhu, M.; Li, J.; Fink, A. L. The Association of Alpha-Synuclein With Membranes Affects Bilayer Structure, Stability, and Fibril Formation. *J. Bio. Chem.* **2003**, *278*, 40186–40197.
- (10) Cholak, E.; Bucciarelli, S.; Bugge, K.; Vestergaard, N. T. J. B.; Arleth, L.; Kragelund, B. B.; Langkilde, A. E. Distinct α -Synuclein:Lipid Co-Structure Complexes

- Affect Amyloid Nucleation Through Fibril Mimetic Behavior. *Biochemistry* **2019**, *58*, 5052–5065.
- (11) Chaudhary, H.; Stefanovic, A. N. D.; Subramaniam, V.; Claessens, M. M. A. E. Membrane interactions and fibrillization of α -synuclein play an essential role in membrane disruption. *FEBS Lett* **2014**, *588*, 4457–4463.
- (12) Varkey, J.; Isas, J. M.; Mizuno, N.; Jensen, M. B.; Bhatia, V. K.; Jao, C. C.; Petrlova, J.; Voss, J. C.; Stamou, D. G.; Steven, A. C.; Langen, R. Membrane curvature induction and tubulation are common features of synucleins and apolipoproteins. *Journal of Biological Chemistry* **2010**, *285*, 32486–32493.
- (13) Pandey, A. P.; Haque, F.; Rochet, J.-C.; Hovis, J. S. α -Synuclein-induced tubule formation in lipid bilayers. *The Journal of Physical Chemistry B* **2011**, *115*, 5886–5893.
- (14) Mizuno, N.; Varkey, J.; Kegulian, N. C.; Hegde, B. G.; Cheng, N.; Langen, R.; Steven, A. C. Remodeling of lipid vesicles into cylindrical micelles by α -synuclein in an extended α -helical conformation. *Journal of Biological Chemistry* **2012**, *287*, 29301–29311.
- (15) Jiang, Z.; D.Flynn, J.; Jr, W. E. T.; Gawrisch, K.; Lee, J. C. Stimulation of α -synuclein amyloid formation by phosphatidylglycerol micellar tubules. *BBA- Biomembranes* **2018**, *1860*, 1840–1847.
- (16) Varkey, J.; Mizuno, N.; Hegde, B. G.; Cheng, N.; Steven, A. C.; Langen, R. α -Synuclein oligomers with broken helical conformation form lipoprotein nanoparticles. *Journal of Biological Chemistry* **2013**, *288*, 17620–17630.
- (17) Eichmann, C.; Campioni, S.; Kowal, J.; Maslennikov, I.; Gerez, J.; Liu, X.; Verasdonck, J.; Nespovitaya, N.; Choe, S.; Meier, B. H.; Picotti, P.; Rizo, J.; Stahlberg, H.; Riek, R. Preparation and Characterization of Stable α -Synuclein Lipoprotein Particles. *J Biol Chem* **2016**, *291*, 8516–8527.

- (18) Viennet, T.; Wördehoff, M. M.; Uluca, B.; Poojari, C.; Shaykhalishahi, H.; Willbold, D.; Strodel, B.; Heise, H.; Buell, A. K.; Hoyer, W.; Etzkorn, M. Structural insights from lipid-bilayer nanodiscs link α -Synuclein membrane-binding modes to amyloid fibril formation. *Communications biology* **2018**, *1*, 44.
- (19) Stöckl, M.; Claessens, M. M. A. E.; Subramaniam, V. Kinetic measurements give new insights into lipid membranepermeabilization by α -synuclein oligomers. *Mol. BioSyst.* **2012**, *8*, 338–345.
- (20) Lorenzen, N.; Nielsen, S. B.; Buell, A. K.; Kaspersen, J. D.; Arosio, P.; Vad, B. S.; Paslawski, W.; Christiansen, G.; Valnickova-Hansen, Z.; Andreasen, M.; Enghild, J. J.; Pedersen, J. S.; Dobson, C. M.; Knowles, T. P. J.; Otzen, D. E. The Role of Stable α -Synuclein Oligomers in the Molecular Events Underlying Amyloid Formation. *J Am Chem Soc* **2014**, *136*, 3859–3868.
- (21) Ghio, S.; Camilleri, A.; Caruana, M.; Ruf, V. C.; Schmidt, F.; Leonov, A.; Ryazanov, S.; Griesinger, C.; Cauchi, R. J.; Kamp, F.; Giese, A.; Vassallo, N. Cardiolipin Promotes Pore-Forming Activity of Alpha-Synuclein Oligomers in Mitochondrial Membranes. *ACS Chem Neurosc* **2019**, *10*, 3815–3829.
- (22) Galvagnion, C.; Buell, A. K.; Meisl, G.; Michaels, T. C. T.; Vendruscolo, M.; Knowles, T. P. J.; Dobson, C. M. Lipid vesicles trigger α -synuclein aggregation by stimulating primary nucleation. *Nat Chem Biol* **2015**, *11*, 229–234.
- (23) Chaudhary, H.; Subramaniam, V.; Claessens, M. M. A. E. Direct Visualization of Model Membrane Remodeling by α -Synuclein Fibrillization. *ChemPhysChem* **2017**, *18*, 1620–1626.
- (24) Galvagnion, C.; Topgaard, D.; Makasewicz, K.; Buell, A. K.; Linse, S.; Sparr, E.; Dobson, C. M. Lipid Dynamics and Phase Transition within α -Synuclein Amyloid Fibrils. *J Phys Chem Lett* **2019**, *10*, 7872–7877.

- (25) Frieg, B.; Antonschmidt, L.; Dienemann, C.; Geraets, J. A.; Najbauer, E. E.; Matthes, D.; de Groot, B. L.; Andreas, L. B.; Becker, S.; Griesinger, C.; F, S. G. The 3D structure of lipidic fibrils of α -synuclein. *Nature Communications* **2022**, *13*, 6810.
- (26) Galvagnion, C.; Brown, J. W. P.; Ouberai, M. M.; Flagmeier, P.; Vendruscolo, M.; Buell, A. K.; Sparr, E.; Dobson, C. M. Chemical properties of lipids strongly affect the kinetics of the membrane-induced aggregation of α -synuclein. *Proceedings of the National Academy of Sciences of the United States of America* **2016**, *113*, 7065–7070.
- (27) Baldwin, A. J.; Knowles, T. P. J.; Tartaglia, G. G.; Fitzpatrick, A. W.; Devlin, G. L.; Shammash, S. L.; Waudby, C. A.; Mossuto, M. F.; Meehan, S.; Gras, S. L.; Christodoulou, J.; Anthony-Cahill, S. J.; Barker, P. D.; Vendruscolo, M.; Dobson, C. M. Metastability of native proteins and the phenomenon of amyloid formation. *J Am Chem Soc* **2011**, *133*, 14160–14163.
- (28) van Gils, J. H. M.; van Dijk, E.; Peduzzo, A.; Hofmann, A.; Vettore, N.; Schützmann, M. P.; Groth, G.; Mouhib, H.; Otzen, D. E.; Buell, A. K.; Abeln, S. The hydrophobic effect characterises the thermodynamic signature of amyloid fibril growth. *PLOS Computational Biology* **2020**, *16*, e1007767.
- (29) Agerschou, E. D. et al. An engineered monomer binding-protein for α -synuclein efficiently inhibits the proliferation of amyloid fibrils. *eLife* **2019**, *8*, e46112.
- (30) Panine, P.; Finet, S.; Weiss, T.; Narayanan, T. Probing fast kinetics in complex fluids by combined rapid mixing and small-angle X-ray scattering. *Adv Coll Interf Sc* **2006**, *127*, 9–18.
- (31) Haertlein, M.; Moulin, M.; Devos, J. M.; Laux, V.; Dunne, O.; Forsyth, V. T. *Methods in enzymology*; Elsevier, 2016; Vol. 566; pp 113–157.

- (32) SH, S. et al. Lewy pathology in Parkinson’s disease consists of crowded organelles and lipid membranes. *Nat Neurosci. Jul;22(7):1099-1109. doi: 10.1038/s41593-019-0423-2. Epub 2019 Jun 24. PMID: 31235907. 2019, 22, 1099–1109.*
- (33) Glatter, O. A new method for the evaluation of small-angle scattering data. *J. Appl. Crystallogr. 1977, 10, 415–421.*
- (34) Pedersen, J. S. Analysis of small-angle scattering data from colloids and polymer solutions: Modeling and least-squares fitting. *Adv. Colloid Interface Sci. 1997, 70, 171–210.*
- (35) Pedersen, M. C.; Arleth, L.; Mortensen, K. WillItFit: a framework for fitting of constrained models to small-angle scattering data. *Journal of Applied Crystallography 2013, 46, 1894–1898.*
- (36) Armen, R. S.; Uitto, O. D.; Feller, S. E. Phospholipid component volumes: Determination and application to bilayer structure calculations. *Biophys. J. 1998, 75, 734–744.*
- (37) Petrache, H. I.; Tristram-Nagle, S.; Gawrisch, K.; Harries, D.; Parsegian, V. A.; Nagle, J. F. Structure and Fluctuations of Charged Phosphatidylserine Bilayers in the Absence of Salt. *Biophysical Journal 2004, 86, 1574–1586.*
- (38) Eichmann, C.; Bibow, S.; Riek, R. α -Synuclein lipoprotein nanoparticles. *Nanotechnol Rev 2017, 6, 105–110.*
- (39) Skar-Gislinge, N.; Simonsen, J. B.; Mortensen, K.; Feidenhans’l, R.; Sligar, S. G.; Lindberg Møller, B.; Bjørnholm, T.; Arleth, L. Elliptical structure of phospholipid bilayer nanodiscs encapsulated by scaffold proteins: Casting the roles of the lipids and the protein. *Journal of the American Chemical Society 2010, 132, 13713–13722.*
- (40) Skar-Gislinge, N.; Arleth, L. Small-angle scattering from phospholipid nanodiscs: Derivation and refinement of a molecular constrained analytical model form factor. *Physical Chemistry Chemical Physics 2011, 13, 3161–3170.*

- (41) Arleth, L.; Vermehren, C. An analytical model for the small-angle scattering of polyethylene glycol-modified liposomes. *Journal of Applied Crystallography* **2010**, *43*, 1084–1091.
- (42) Kohn, J. E.; Millett, I. S.; Jacob, J.; Zagrovic, B.; Dillon, T. M.; Cingel, N.; Dothager, R. S.; Seifert, S.; Thiyagarajan, P.; Sosnick, T. R., et al. Random-coil behavior and the dimensions of chemically unfolded proteins. *Proceedings of the National Academy of Sciences* **2004**, *101*, 12491–12496.
- (43) Lund, R.; Willner, L.; Richter, D.; Lindner, P.; Narayanan, T. Kinetic Pathway of the Cylinder-to-Sphere Transition in BlockCopolymer Micelles Observed in Situ by Time-Resolved Neutron and Synchrotron Scattering. *ACS Macro Lett* **2013**, *2*, 1082–1087.
- (44) von Smoluchowski, M. Versuch einer mathematischen Theorie der Koagulationskinetik kolloider Lösungen. *Zeitschrift für Physikalische Chemie* **1917**, *92*, 129.
- (45) Wolff, M.; Mittag, J. J.; Herling, T. W.; Genst, E. D.; Dobson, C. M.; Knowles, T. P. J.; Braun, D.; Buell, A. K. Quantitative thermophoretic study of disease-related protein aggregates. *Scientific reports* **2016**, *6*, 22829.
- (46) Vijayakumar, M.; Wong, K.-Y.; Schreiber, G.; Fersht, A.; Szabo, A.; Zhou, H.-X. Electrostatic Enhancement of Diffusion-controlled Protein-Protein Association: Comparison of Theory and Experiment on Barnase and Barstar. *J Mol Biol* **1998**, *278*, 1015–1024.
- (47) Galvagnion, C. The Role of Lipids Interacting with α -Synuclein in the Pathogenesis of Parkinson's Disease. *Journal of Parkinson's Disease* **2017**, *7*, 433–450.
- (48) Zhang, X.; St. Clair, J. R.; London, E.; Raleigh, D. P. Islet amyloid polypeptide membrane interactions: effects of membrane composition. *Biochemistry* **2017**, *56*, 376–390.

- (49) Habchi, J.; Chia, S.; Galvagnion, C.; Michaels, T. C. T.; Bellaiche, M. M. J.; Ruggeri, F. S.; Sanguanini, M.; Idini, I.; Kumita, J. R.; Sparr, E.; Linse, S.; Dobson, C. M.; Knowles, T. P. J.; Vendruscolo, M. Cholesterol catalyses A β 42 aggregation through a heterogeneous nucleation pathway in the presence of lipid membranes. *Nature chemistry* **2018**,
- (50) Rabe, M.; Soragni, A.; Reynolds, N. P.; Verdes, D.; Liverani, E.; Riek, R.; Seeger, S. On-surface aggregation of α -synuclein at nanomolar concentrations results in two distinct growth mechanisms. *ACS Chem Neurosci* **2013**, *4*, 408–417.
- (51) Banerjee, S.; Hashemi, M.; Zagorski, K.; Lyubchenko, Y. L. Cholesterol in membranes facilitates aggregation of amyloid β protein at physiologically relevant concentrations. *ACS Chemical Neuroscience* **2021**, *12*, 506–516.
- (52) Lautenschläger, J.; Stephens, A. D.; Fusco, G.; Ströhl, F.; Curry, N.; Zacharopoulou, M.; Michel, C. H.; Laine, R.; Nespovitaya, N.; Fantham, M., et al. C-terminal calcium binding of α -synuclein modulates synaptic vesicle interaction. *Nature communications* **2018**, *9*, 1–13.
- (53) Hoover, B. M.; Shen, Z.; Gahan, C. G.; Lynn, D. M.; Van Lehn, R. C.; Murphy, R. M. Membrane remodeling and stimulation of aggregation following α -synuclein adsorption to phosphatidylserine vesicles. *The Journal of Physical Chemistry B* **2021**, *125*, 1582–1594.
- (54) Hellstrand, E.; Nowacka, A.; Topgaard, D.; Linse, S.; Sparr, E. Membrane lipid coaggregation with α -synuclein fibrils. *PLoS One* **2013**, *8*, e77235.
- (55) van Maarschalkerweerd and Valeria Vetri and Annette Eva Langkilde and Vito Foderà and Bente Vestergaard, A. Protein/Lipid Coaggregates are Formed During α -Synuclein-Induced Disruption of Lipid Bilayers. *Biomacromolecules* **2014**, *15*, 3643–3654.

- (56) Fridolf, S.; Pham, Q. D.; Pallbo, J.; Bernfur, K.; Linse, S.; Topgaard, D.; Sparr, E. Ganglioside GM3 stimulates lipid-protein co-assembly in α -synuclein amyloid formation. *Biophys Chem* **2022**, *293*, 106934.
- (57) Haertlein, M.; Moulin, M.; Devos, J. M.; Laux, V.; Dunne, O.; Trevor Forsyth, V. In *Methods in Enzymology*; Kelman, Z., Ed.; Isotope Labeling of Biomolecules - Applications; Academic Press, 2016; Vol. 566; pp 113–157.
- (58) Narayanan, T.; Gummel, J.; Gradzielski, M. In *Probing the Self-Assembly of Unilamellar Vesicles Using Time-Resolved SAXS*; Iglič, A., Kulkarni, C. V., Eds.; Advances in Planar Lipid Bilayers and Liposomes; Academic Press, 2014; Vol. 20; pp 171–196.
- (59) Galvagnion, C.; Buell, A. K.; Dobson, C.; Martel, A.; Roosen-Runge, F. Real-time monitoring of the change in lipid vesicle structure upon amyloid fibril formation. 2015; Institut Laue-Langevin (ILL), doi:10.5291/ILL-DATA.8-02-754.
- (60) Galvagnion, C.; Buell, A. K.; Dobson, C.; Martel, A.; Porcar, L.; Roosen-Runge, F. Structural investigation of early protein-lipid coaggregates. 2015; Institut Laue-Langevin (ILL), doi:10.5291/ILL-DATA.8-03-874.